

The Spectral Energy Distributions of Low-Luminosity Active Galactic Nuclei

Luis C. Ho¹

Harvard-Smithsonian Center for Astrophysics, 60 Garden St., Cambridge, MA 02138

ABSTRACT

As a step toward elucidating the physical conditions in nearby active galaxies, this paper presents spectral energy distributions (SEDs) of a sample of seven low-luminosity active galactic nuclei (AGNs). SEDs for four objects are presented for the first time (NGC 4261, NGC 4579, NGC 6251, and M84); the data for the remaining three (M81, M87, and NGC 4594) have been substantially updated compared to previous studies. The nuclear fluxes were carefully selected so as to avoid contamination by emission from the host galaxy, which can be substantial for very weak nuclei.

The present sample of low-luminosity nuclei all exhibit SEDs that look markedly different from the canonical broad-band continuum spectrum of luminous AGNs. The most striking difference is that the low-luminosity objects lack an ultraviolet excess (the “big blue bump”), a feature normally associated with emission from a standard optically thick, geometrically thin accretion disk. The weakness of the ultraviolet band leads to an unusually steep optical-ultraviolet continuum shape and a more pronounced contribution from the X-rays to the ionizing spectrum. It is argued that the absence of the big blue bump is a property intrinsic to the SEDs and not an artifact of strong dust extinction. Another notable property of the SEDs is the prominence of the compact, flat-spectrum radio component relative to the emission in other energy bands. All seven nuclei in the sample, including three hosted by spiral galaxies, technically qualify as “radio-loud” objects according to conventional criteria. Finally, the integrated spectra confirm the exceptional weakness of the nuclei: the bolometric luminosities range from 2×10^{41} to 8×10^{42} ergs s⁻¹, or $\sim 10^{-6} - 10^{-3}$ times the Eddington rate for the black hole masses previously reported for these galaxies.

Subject headings: galaxies: active — galaxies: nuclei — galaxies: Seyfert

1. Introduction

The spectral energy distributions (SEDs) of active galactic nuclei (AGNs) carry important information on the physical processes of the accretion process. Many aspects of the AGN

¹Current address: Carnegie Observatories, 813 Santa Barbara St., Pasadena, CA 91101-1292.

phenomenon, including the SED, have been successfully interpreted within the accretion disk framework, specifically one in which the disk is assumed to be optically thick and physically thin (Blandford & Rees 1992, and references therein). Previous work, however, has concentrated nearly exclusively on high-luminosity AGNs — mainly bright Seyfert nuclei and QSOs. Very little data exist on the spectral properties of low-luminosity AGNs, such as those commonly found in nearby galaxies (Ho, Filippenko, & Sargent 1997a), because they are difficult to study. Yet, knowledge of the SEDs of AGNs in the low-luminosity regime is fundamental to understanding the physical nature of these objects and their relation to their more luminous counterparts.

The intrinsic weakness of low-luminosity nuclei poses practical challenges on obtaining the data. Aside from the issue of sensitivity, often the main limitation stems from insufficient angular resolution necessary to separate the faint central source from the galaxy background. At virtually all wavelengths of interest the core emission constitutes only a small fraction of the total light, and hence contamination from the host galaxy is severe. To date, only a handful of objects have been adequately studied with multiwavelength observations, and even for these the wavelength coverage is sometimes highly incomplete and the data only approximate (NGC 1316 and NGC 3998: Fabbiano, Fasnacht, & Trinchieri 1994; Sgr A*: Narayan, Yi, & Mahadevan 1995; M81: Ho, Filippenko, & Sargent 1996; NGC 4258: Lasota et al. 1996; M87: Reynolds et al. 1996; NGC 4594: Fabbiano & Juda 1998, Nicholson et al. 1998). Nonetheless, these studies already suggest that the SEDs of low-luminosity AGNs look markedly different compared to the SEDs normally seen in luminous AGNs. The spectral peculiarities seen in low-luminosity AGNs hint at possibly significant departures in these objects from the standard AGN accretion disk model.

This paper presents SEDs for a small sample of low-luminosity AGNs for which reasonably secure black hole masses have been determined by dynamical measurements. Data are presented for a total of seven objects (see Table 1 for a summary), four for the first time (NGC 4261, NGC 4579, NGC 6251, and M84); the SEDs for the remaining three (M81, M87, and NGC 4594) have been substantially updated and improved compared to previous publications. The sample consists of four objects spectroscopically classified as low-ionization nuclear emission-line regions or LINERs (Heckman 1980; see Ho 1999a for a review), one Seyfert, and two objects that border on the definition of LINERs and Seyferts. It is worth remarking that, although the sample is admittedly small and heterogeneous, it contains *every* known low-luminosity object that has both a black hole mass determination and sufficient multiwavelength data to establish the SED. The only two not included, namely Sgr A* and NGC 4258, have already been extensively discussed in the literature. Because of the many complexities (§ 2) involved in defining the nuclear SEDs of these weak sources, because so few data of this kind exist in the literature, and because a companion paper (Ho et al. 1999b) relies critically on the details presented here, I devote considerable attention in § 2 to describing the data selection for each object. Section 3 summarizes the most noteworthy trends observed collectively in the sample, and section 4 discusses possible complications introduced by dust extinction; readers not interested in the details of each object may wish to skip directly to sections 3 and 4 for an overview of the main results. Ho et al. (1999b)

will present detailed modeling of these data based on accretion-disk calculations.

2. Compilation of the Data

As mentioned in § 1, measuring the weak signal from low-luminosity AGNs requires observations that minimize the contamination from the bright background of the host galaxy. High angular resolution, therefore, is indispensable at all wavelengths. This study takes the following strategy for data selection. (1) At radio wavelengths, only interferometric data will be used, preferably measured through VLBI techniques. The radio jet component, if present, potentially can contaminate the core emission even in sub-arcsecond resolution. (2) Data in the infrared (IR) window are at the moment most poorly constrained. There are no useful far-IR data because nearly all the existing measurements have been obtained using the *Infrared Astronomical Satellite*, which has a beam $\gtrsim 1'$. Ground-based measurements in the mid-IR (10–20 μm) and near-IR (1–3 μm) are widely available in the literature, but these data should be regarded strictly as upper limits because of the relatively large apertures employed ($\sim 3''$ – $10''$). The energy distribution of normal stellar populations implies that the contamination from starlight in the near-IR should greatly exceed that in the mid-IR; thus, the mid-IR points should be more representative of the direct emission from the nucleus, although emission from hot (~ 100 K) dust grains can substantially boost the luminosity in this band (e.g., Willner et al. 1985). (3) All of the optical and ultraviolet (UV) data are derived from observations made with the *Hubble Space Telescope* (*HST*). Photometry points generally pertain to an aperture of $\sim 0''.1$, while apertures $\lesssim 1''$ have been used for spectroscopic measurements. (4) Finally, I quote only X-ray fluxes that originate from a nuclear source known to be compact at soft X-ray energies (0.5–2.5 keV). The criterion for compactness, unless otherwise noted, is currently limited to the resolution of the High-Resolution Imager (HRI), approximately $\sim 5''$, on either the *Einstein* or the *ROSAT* satellite. Several objects have hard X-ray (2–10 keV) spectra acquired with *ASCA*, which has an angular resolution of $\sim 5'$; HRI images show that the soft X-ray emission is compact in all these cases.

The following subsections describe the data chosen for each object. Additional details can be found in Tables 2–8, and the individual SEDs are shown in Figures 1–7.

2.1. NGC 3031 (M81)

The SED presented in Ho et al. (1996) has been updated (Table 2; Fig. 1) with new optical and UV photometry points from *HST*, an additional high-frequency radio point, and a more up-to-date hard X-ray spectrum from *ASCA*. The radio continuum between ~ 1 and 15 GHz shows an inverted spectrum ($\alpha \approx -0.3$ to -0.6 , where $F_\nu \propto \nu^{-\alpha}$). It is difficult to assess the reality of the apparent slight turnover between 5 and 15 GHz because the two data points were not observed simultaneously; the radio core of M81 is highly variable on many timescales (Ho et al. 1999a). The

spectroscopically measured optical–UV slope of the featureless continuum is surprisingly steep. Even after accounting for an estimated reddening of $E(B - V) = 0.094$ mag, the slope is still ~ 2 (Ho et al. 1996). Devereux, Ford, & Jacoby (1997) recently obtained an *HST* WFPC2 image of the nucleus of M81 using a filter centered near 1500 Å. They obtained a flux ~ 4 times higher than that reported in the Faint Object Spectrograph (FOS) UV spectrum of Ho et al. (1996). The two new points based on optical images (Bower et al. 1996; Devereux et al. 1997), on the other hand, are consistent with the spectroscopic measurements. Maoz et al. (1998) have reanalyzed the FOS UV data and concluded that the nucleus may have been miscentered in the aperture during the observations. This may account for the discrepancy between the FOS and WFPC2 fluxes, although it cannot be excluded that the nucleus varied in the UV between the two observing epochs. Adopting the WFPC2 UV flux, the optical–UV slope is now $\alpha \approx 1.3$ – 1.4 . The nucleus of M81 emits a nonthermal continuum in the hard X-ray band. The spectrum between 2–10 keV is well described by a single power law with a slope of $\alpha = 0.85 \pm 0.04$ (Ishisaki et al. 1996; see also Serlemitsos, Ptak, & Yaqoob 1996), similar to that seen in luminous Seyfert 1 nuclei (Turner & Pounds 1989; Nandra et al. 1997); the luminosity in this case, however, is just 2×10^{40} ergs s^{-1} . It is noteworthy that M81 emits substantially more energy in the X-rays relative to the UV than in luminous AGNs. The two-point spectral index between 2500 Å and 2 keV, α_{ox} , is 1.08, smaller than the average value in quasars (1.4) or in luminous Seyfert 1 nuclei (1.2) (Mushotzky & Wandel 1989).

2.2. NGC 4261 (3C 270)

Figure 2 (Table 3) displays the SED of the nucleus. The radio core is resolved even on a scale of several milliarcseconds. No obvious point source can be seen in the 1.6 and 8.4 GHz maps of Jones & Wehrle (1997), so I take as a reasonable approximation the peak intensities at these frequencies. The resulting radio spectrum has $\alpha = 0$. The three optical points derived from WFPC2 images (Ferrarese, Ford, & Jaffe 1996) define a slope of $\alpha \approx 2.2$. The FOS spectrum of Ferrarese et al., taken with a similar-sized aperture ($0''.1$), suggests that most of the continuum is nonstellar. The very steep optical continuum probably results mainly from reddening by dust internal to NGC 4261 and most likely associated with the nuclear disk. Patchy extinction can be seen throughout the disk and in the immediate vicinity of the nucleus (Ferrarese et al. 1996). Dust is also the most likely culprit for the complete absence of UV emission: the upper limit to the flux at 2300 Å is 10^{-16} ergs s^{-1} cm^{-2} (Zirbel & Baum 1998), a factor of 80 lower than expected from a simple power-law extrapolation of the observed optical continuum. Estimating the intrinsic optical and UV luminosity of the nucleus, however, is difficult without prior knowledge of the absorbing column, the source geometry, and the extinction law (see § 4). The extinction due to the Galaxy is small. The foreground hydrogen column density is only $N_{\text{H}} = 1.6 \times 10^{20}$ cm^{-2} , which, for the conversions $E(B - V) = N_{\text{H}} / (5.8 \times 10^{21} \text{ cm}^{-2})$ mag and $A_V / E(B - V) = 3.1$ (Bohlin, Savage, & Drake 1978), translates to $A_V = 0.084$ mag (Table 1). A rough estimate of the magnitude of the internal extinction can be obtained from the Balmer decrement observed through a larger aperture

($2'' \times 4''$) by Ho et al. (1997b), $H\alpha/H\beta = 4.9$.² After removing the Galactic contribution using the extinction law of Cardelli, Clayton, & Mathis (1989), $H\alpha/H\beta(\text{internal}) = 4.8$; assuming the Galactic extinction law and a Case B' intrinsic $H\alpha/H\beta$ of 3.1, which is thought to be appropriate for the conditions in the narrow-line regions of AGNs (e.g., Gaskell & Ferland 1984), $A_V(\text{internal}) = 1.4$ mag. This value is much higher than that inferred from the soft X-ray observations of Worrall & Birkinshaw (1994), who placed a limit of $N_H < 3.9 \times 10^{20} \text{ cm}^{-2}$, or $A_V < 0.2$ mag for a normal dust-to-gas ratio.

Worrall & Birkinshaw (1994) observed NGC 4261 with the *ROSAT* Position-Sensitive Proportional Counter (PSPC). Despite the coarse angular resolution of the PSPC ($\sim 25''$), they found that $\sim 50\%$ of the flux comes from a spatially unresolved component whose spectrum is well fitted by a power-law function. The nonthermal component emits $L(0.2\text{--}1.9 \text{ keV}) = 4.7 \times 10^{40} \text{ ergs s}^{-1}$. Inspection of an archival *ROSAT* HRI image confirms that most of the soft X-ray emission indeed does stem from a compact component. The uncertain impact of dust extinction on the optical-UV continuum renders estimates of α_{ox} highly unreliable. If $A_V(\text{internal}) = 0$ mag (correcting only for the Galactic contribution), the optical slope is $\alpha = 2.06$, which, when extrapolated to 2500 \AA yields $\alpha_{\text{ox}} = 0.44$. Choosing $A_V(\text{internal}) = 1.4$ mag and the Galactic extinction law, the optical slope becomes $\alpha = 0.67$, and $\alpha_{\text{ox}} = 0.84$. These two extremes probably bracket the true value.

2.3. NGC 4374 (M84, 3C 272.1)

Jones, Terzian, & Sramek (1981) mapped the nucleus with a resolution of 4 mas at 1.6 GHz. The morphology of the radio core can be modeled by an elliptical Gaussian with dimensions $1.4 \text{ mas} \times 6.0 \text{ mas}$, presumably because a parsec-scale jet still contributes to the emission on these scales. The radio flux from the accretion flow, therefore, ought to be less than indicated in Figure 3 (Table 4). At optical wavelengths the nucleus appears unresolved in WFPC2 images. Bower et al. (1997) measure $V = 19.9$ mag and $(V - I) = 1.6$ mag. The stellar contribution to the pointlike nucleus is unclear, but judging from the complete absence of stellar absorption features between 6300 \AA and 6800 \AA in spectra acquired through a $0''.2$ slit (Bower et al. 1998), most of the light is probably nonstellar. The ground-based spectrum in Ho et al. (1995), for instance, shows a very noticeable (equivalent width $\sim 1 \text{ \AA}$) absorption line at $\lambda = 6495 \text{ \AA}$ due to Ca I+Fe I. The $(V - I)$ color of the nucleus, which corresponds to $\alpha = 3.5$, again suggests substantial reddening by dust, as does the nondetection of UV emission (Zirbel & Baum 1998); the images in Bower et al. (1997), in fact, clearly show dust patches projected on the front of the nucleus. These authors used the

²Ferrarese et al. (1996) quote a significantly larger value of $H\alpha/H\beta = 9.7$. Comparison of their relative line intensities with those of Ho et al. (1997b) suggests that they have underestimated the intensity of $H\beta$ by a factor of ~ 2 . Ferrarese et al. could not remove the underlying stellar absorption lines from their spectra because of the limited signal-to-noise ratio of their data. This effect preferentially biases the Balmer line intensities, $H\beta$ more so than $H\alpha$, to low values.

($V - I$) color map and an assumed intrinsic ($V - I$) color for ellipticals to estimate a mean internal extinction of $A_V = 0.54$ mag within a relatively large region of $14''.5 \times 8''.4$. Close to the nucleus the extinction could be higher than this value. The intrinsic Balmer decrement measured through a $2'' \times 4''$ aperture around the nucleus, for instance, is $H\alpha/H\beta = 4.7$ (Ho et al. 1997b), or $A_V = 1.3$ mag. The optical and UV points were dereddened using this A_V .

The *Einstein* HRI image of M84 reveals a relatively complex central morphology with significant extended emission (Fabbiano, Kim, & Trinchieri 1992); the extended structure is also clearly evident in an archival *ROSAT* HRI image. The 0.5–4 keV luminosity given by Fabbiano et al. (1992), 5.3×10^{40} ergs s $^{-1}$ (assuming a “Raymond-Smith” thermal spectrum with $kT = 1$ keV and a line-of-sight $N_H = 1.7 \times 10^{20}$ cm $^{-2}$), should be taken only as an upper limit to the luminosity of a pointlike nucleus. Extrapolating the $\alpha \approx 3.1$ optical slope to the UV gives an estimate of $\alpha_{\text{ox}} \approx 0.75$.

2.4. NGC 4486 (M87, 3C 274)

Reynolds et al. (1996) presented a sparse SED for the nucleus. Figure 4 (Table 5) gives an updated version that includes additional data from the IR to UV region. As in the objects discussed so far, the radio spectrum is either flat or slightly inverted; the VLBI points (filled symbols) have a mean spectral index $\langle \alpha \rangle \approx 0.1$. The apparent change in the spectral index from one point to another reflects the nonuniform resolution of the four experiments, which results in varying degrees of contamination from the jet, the nonsimultaneity of the observations, or both. It is instructive to note that the jet in this case introduces very substantial contamination to the radio core emission even on a scale of $\sim 1''$. The open symbols show the three VLA points from Biretta, Stern, & Harris (1991); clearly they lie systematically higher by about a factor of 10 compared to the VLBI flux densities. The optical (6800 Å) to UV (1200 Å) spectrum, observed nearly simultaneously with the *HST*/FOS through the same ($0''.2$) aperture, traces a smooth, continuous curve that can be well fitted with a double power law ($\alpha = 1.75$ for $\lambda \lesssim 4500$ Å, $\alpha = 1.41$ for $\lambda \gtrsim 4500$ Å; Tsvetanov et al. 1998). The two *I*-band points derived from archival *HST* images agree very well with the FOS spectrum (within $\pm 10\%$). On the other hand, the point taken from the Faint Object Camera (FOC) measurement of Maoz et al. (1995) is about 50% higher than predicted from the FOS spectrum; variability is a plausible explanation for this discrepancy. The fluxes in the *J* ($1.25\mu\text{m}$) and *K* ($2.2\mu\text{m}$) bands (Stiavelli, Peletier, & Carollo 1997), both acquired under sub-arcsecond seeing conditions, also appear to follow the extrapolated optical power law. Taken at face value, the $10\mu\text{m}$ point deviates quite strongly from the power law at shorter wavelengths, but the relatively large aperture of the observations ($6''$) allows room for substantial contamination. The soft X-ray flux recorded by the *Einstein* HRI is $\sim 50\%$ lower than that seen in the *ROSAT* HRI [$L(1 \text{ keV}) = 5.4 \times 10^{40}$ ergs s $^{-1}$, assuming a power-law spectrum with $\alpha = 0.7$ and a line-of-sight $N_H = 2.5 \times 10^{20}$ cm $^{-2}$; see Reynolds et al. 1996]. This level of long term X-ray variability is not uncommon in low-luminosity AGNs (Serlemitsos et al. 1996). An

ASCA spectrum of M87 is available, but the nucleus could not be clearly detected in the relatively short exposure (Reynolds et al. 1996). Combining the UV spectrum with the average of the two HRI fluxes, $\alpha_{\text{ox}} = 1.06$.

M87 belongs to the minority of LINERs ($\sim 25\%$; Maoz et al. 1995; Barth et al. 1998) that shows prominent UV emission. The optical-UV continuum of M87 evidently suffers little or no internal extinction. The best-fitting double power-law model shown in Figure 4 requires only $A_V = 0.12$ mag for a Milky Way extinction law (Tsvetanov et al. 1998), very similar to the Galactic contribution of $A_V = 0.078$ mag. Note that the Balmer decrement measured by Ho et al. (1997b) in a $2'' \times 4''$ aperture yields a substantially larger A_V of 1.0 mag. This example underscores the dangers of comparing observations taken with markedly different apertures.

2.5. NGC 4579 (M58)

The 2.3-GHz and 8.4-GHz interferometric observations of Sadler et al. (1995), both made with a beam of $0''.03$, define a rising radio spectrum with $\alpha = -0.19$ (Fig. 5; Table 6). The *HST*/FOS UV spectrum of Barth et al. (1996) extends from $\sim 3300 \text{ \AA}$ to 1150 \AA ; excluding a broad feature near 3000 \AA due to Balmer continuum and Fe II emission, the spectrum can be described by a nearly featureless power-law function, $F_\nu \propto \nu^{-1}$. There is tentative evidence that the nucleus varies in the UV. The 2300 \AA flux in the FOS spectrum is a factor of 3 lower than that reported by Maoz et al. (1995) based on an FOC image. In either case, the UV output, again, is quite low with respect to the X-rays: $\alpha_{\text{ox}} = 0.78$ and 1.02 for the FOS and FOC UV flux, respectively. A compact, nonthermal component dominates the *ASCA* spectrum of NGC 4579. Terashima et al. (1998) find that the 2–10 keV continuum can be modeled as a moderately absorbed (intrinsic $N_{\text{H}} = 4 \times 10^{20} \text{ cm}^{-2}$) power law with $\alpha = 0.72$ and luminosity $1.5 \times 10^{41} \text{ ergs s}^{-1}$. The value of N_{H} derived from the X-ray spectrum roughly matches the intrinsic extinction estimated by Barth et al. (1996) based on the shape of the observed UV continuum.

2.6. NGC 4594 (M104, Sombrero)

Fabbiano & Juda (1997) presented an approximate SED for the nucleus of NGC 4594. The optical and UV points used in that study, however, were highly uncertain. The *B*-band data, based on the pre-refurbishment FOC image of Crane et al. (1993), may have been underestimated because of the nonlinear behavior of the FOC (see Crane & Vernet 1997). On the other hand, the UV flux taken with the very large aperture ($10'' \times 20''$) of the *International Ultraviolet Explorer* is undoubtedly far too high. Here the SED of NGC 4594 is reassessed, paying close attention to aperture effects in the difficult optical-UV region; a preliminary version of these data appears in Nicholson et al. (1998).

The high-resolution data between 0.6 and 15 GHz define a compact flat-spectrum core with

α ranging from 0.2 to -0.4 (Fig. 6; Table 7). The nonstellar component of the optical and UV continuum, on the other hand, is somewhat difficult to specify. The optical FOS spectrum of Kormendy et al. (1997), taken through a $0''.21$ aperture, has a very red continuum ($\alpha \approx 3.5$). The steep optical slope is most likely caused by an increasing contamination of starlight toward longer wavelengths (even within such a small aperture) rather than by dust reddening of a purely featureless continuum. The dilution of the depth of the stellar absorption lines indicated to Kormendy et al. that approximately 50% of the light at B within their $0''.21$ aperture comes from the nonstellar continuum. This roughly agrees with the strength of the point source extracted from an archival WFPC2 V -band image (Table 7). The point-source luminosity similarly measured from an I -band image, however, falls significantly below (by a factor ~ 4) the extrapolated FOS spectrum if one assumes the degree of stellar contamination to be constant between B and I . This suggests that the nonstellar component contributes much less to the red end of the FOS spectrum ($\sim 6800 \text{ \AA}$), probably on the order of 25% or so. The I -band flux is therefore adopted for the red end of the FOS spectrum. If one considers the two photometry points to be a reliable measure of the nonstellar component, the optical slope decreases to $\alpha = 1.3$. The UV spectrum, taken with an even larger aperture of $0''.86$, likewise suffers from wavelength-dependent starlight contamination (Nicholson et al. 1998). I excluded from the SED the portion of the spectrum longward of $\lambda = 2200 \text{ \AA}$, where incipient stellar absorption features and a sharply rising continuum suggest a sizable contribution from stars. The final adopted optical and UV points (shown as filled symbols) are well joined by a power law with $\alpha \approx 1.5$.

The *ASCA* 2–10 keV spectrum is predominantly nonthermal. Nicholson et al. (1998) obtained a best fit with a power law with $\alpha = 0.63$ and $L(2\text{--}10 \text{ keV}) = 1.1 \times 10^{41} \text{ ergs s}^{-1}$. The morphology of the central region as seen in the *ROSAT* HRI image (Fabbiano & Juda 1997) indicates that most of the hard X-ray emission is likely to originate from the nucleus. The X-ray band energetically dominates over the UV band, with $\alpha_{\text{ox}} = 0.89$. The average extinction inferred from the Balmer decrement on arcsecond scales appears modest ($A_V = 0.25 \text{ mag}$; Ho et al. 1997b) and roughly agrees with the intrinsic hydrogen column derived from the *ASCA* spectrum ($N_{\text{H}} = 5.3 \times 10^{20} \text{ cm}^{-2}$ or $A_V = 0.28 \text{ mag}$).

2.7. NGC 6251

Good quality VLBI maps are available to isolate the core radio emission (Cohen & Readhead 1979; Jones et al. 1986), but the nonsimultaneous nature of the observations makes definition of the intrinsic radio spectrum ambiguous (Fig. 7; Table 8). The two low-frequency points, for instance, yield a much steeper spectral index than the two high-frequency points ($\alpha = 0.4$ compared to $\alpha = -1.2$). The only conclusion that can be drawn at this stage is that the radio spectrum, as in all the sources studied here, is consistent with that of a self-absorbed synchrotron source. Four *HST* photometry points have been measured for the pointlike nucleus, corresponding roughly to the U, B, V , and I bands (Crane & Vernet 1997). Taking into consideration the

nonlinear effects of the FOC that affected the U and B fluxes, the optical to near-UV slope is consistent with $\alpha \approx 1.7$. Combining the extrapolated UV flux with the soft X-ray (PSPC) flux reported by Worrall & Birkinshaw (1994), $\alpha_{\text{ox}} = 0.83$. Birkinshaw & Worrall (1993) performed a detailed analysis of the PSPC data and concluded that nearly all ($\sim 90\%$) of the emission arises from a spatially unresolved, power-law component with a diameter $\lesssim 4''$. More detailed spectral information comes from Turner et al.’s (1997) statistical study of the *ASCA* spectra of a large sample of Seyfert 2 nuclei, which included NGC 6251. The best-fitting model found by Turner et al. requires a thermal (Raymond-Smith) plasma with a temperature of $kT = 0.85$ keV added to a power-law component characterized by $\alpha = 1.11^{+0.16}_{-0.19}$, $L(2\text{--}10 \text{ keV}) = 1.3 \times 10^{42} \text{ ergs s}^{-1}$, and an intrinsic $N_{\text{H}} = 1.4 \times 10^{21} \text{ cm}^{-2}$. The absorbing column obtained from the X-rays predicts a sizable internal extinction of $A_V = 0.75$ mag. The Balmer decrement given in Shuder & Osterbrock (1981) requires a much larger $A_V \approx 5$ mag, although the reported $\text{H}\beta$ intensity appears to be rather uncertain.

3. General Properties of the SEDs

Luminous AGNs generally display a fairly “universal” SED (see, e.g., Sanders et al. 1989 and Elvis et al. 1994). The continuum from the IR to the X-rays, roughly flat in $\log \nu F_\nu$ – $\log \nu$ space, can be represented by an underlying power law with $\alpha \approx 1$ superposed with several distinct components, the most prominent of which is a broad UV excess. This so-called big blue bump is conventionally interpreted as thermal emission arising from an optically thick, geometrically thin accretion disk (Shields 1978; Malkan & Sargent 1982). The largest spectral difference among AGNs manifests itself in their brightness in the radio band — a factor of nearly 10^2 – 10^3 in radio power distinguishes “radio-loud” from “radio-quiet” objects.

The broad-band spectra of the seven low-luminosity AGNs presented here share a number of common traits, and yet they differ markedly from the SEDs of luminous AGNs. To illustrate this point, Figure 8 compares the SEDs of the present sample with the median SED of radio-loud and radio-quiet luminous AGNs taken from Elvis et al. (1994); all the curves have been normalized at 1 keV. Several features of the low-luminosity SEDs are noteworthy:

(1) The optical-UV slope is quite steep. The power-law indices for the seven objects average $\alpha \approx 1.8$ (range 1.0–3.1; see Table 9), or 1.5 if the possibly highly reddened objects NGC 4261 and M84 are excluded, whereas in luminous AGNs $\alpha \approx 0.5$ –1.0.

(2) The UV band is exceptionally dim relative to the optical and X-ray bands. There is no evidence for a big blue bump component in any of the objects. Indeed, the SED reaches a local minimum somewhere in the far-UV or extreme-UV region. This leads to the above-mentioned steep optical-UV slope and to systematically low values of α_{ox} . Table 9 gives $\langle \alpha_{\text{ox}} \rangle \approx 0.9$, to be compared with $\langle \alpha_{\text{ox}} \rangle = 1.2$ –1.4 for luminous Seyferts and QSOs (Mushotzky & Wandel 1989). In other words, the low-luminosity AGNs in the present sample, most of which are LINERs, are

systematically “X-ray loud” (relative to the UV) compared to AGNs of higher luminosity. This modification of the SED from UV to X-ray energies leads to a harder ionizing spectrum, and it offers an explanation, at least in part, for the characteristically lower ionization state of the emission-line regions (Ho 1999b).

(3) The hard X-ray (2–10 keV) spectra, where available, are well fitted with a power-law function with $\alpha \approx 0.6$ –0.8, very similar to spectra observed in high-luminosity sources.

(4) There is tentative evidence for a maximum in the SED at mid-IR or longer wavelengths. Despite the relatively large apertures employed in the mid-IR observations, the 10- μ m point should be largely uncontaminated by starlight, although dust emission could contribute significantly in this band.

(5) The nuclei have radio spectra that are either flat or inverted. The radio brightness temperature, where available, reach at least 10^9 – 10^{10} K. The radio cores, therefore, are self-absorbed synchrotron sources.

(6) One usually gauges the degree of radio dominance in AGNs by the ratio of the specific luminosities in the radio to the optical band. For instance, Kellermann et al. (1989) classify the radio strength of QSOs by the parameter $R \equiv F_\nu(6\text{cm})/F_\nu(B)$; radio-quiet members have $R \approx 0.1$ –1, and radio-loud members are distinguished by $R \gtrsim 100$. Adopting the same criterion, *all* of the objects, including the three spiral galaxies in the sample (M81, NGC 4579, and NGC 4594), qualify as being *radio-loud*. M81 has the smallest radio-to-optical ratio, but R is still ~ 50 . This finding runs counter to the usual notion that only elliptical galaxies host radio-loud AGNs. Note that if the total (host galaxy + nucleus) B luminosity had been used, which in these sources significantly exceeds the nuclear value alone, all the objects, with the possible exception of NGC 6251, would have been considered radio quiet.

(7) The sample of objects studied here is intrinsically extremely faint. To cast this statement in a more familiar context and to fully appreciate the enormous challenge in detecting these objects, we note that AGNs that occupy the upper end of the luminosity distribution, namely QSOs, typically have nonstellar continua with absolute magnitudes $-30 < M_B^{nuc} < -23$. Classical Seyfert nuclei, such as those from the Markarian survey, are characterized by $-23 < M_B^{nuc} < -18$. By contrast, the nonstellar nuclear magnitudes listed in Table 9 lie in the range $-14.7 < M_B < -8.9$. Excluding the two extreme cases, $\langle M_B^{nuc} \rangle = -11.5$ mag. The host galaxies themselves, on the other hand, are luminous L^* systems ($\langle M_{BT}^0 \rangle \approx -21.1$ mag; Table 1), and hence the nuclei comprise merely $\sim 0.01\%$ of the total optical light of the host galaxies.

(8) The bolometric luminosities of the sources (Table 9), obtained by integrating the power-law segments shown on Figure 8, range from $L_{\text{bol}} = 2 \times 10^{41}$ to 8×10^{42} ergs s^{-1} , or $\sim 10^{-6}$ – 10^{-3} times the Eddington rate for the black hole masses listed in Table 1. The bolometric luminosities would be lower if the mid-IR peak has been overestimated, but this would not affect the conclusion that the Eddington ratios are very low. The X-ray band, arbitrarily defined here as the region from 0.5 to 10 keV, carries 6%–33% of L_{bol} .

4. Uncertainties due to Dust Extinction

Important aspects of the interpretation of the data depend on the intrinsic luminosity of the UV region, as this impacts conclusions concerning the optical-UV continuum slope, the presence of the big blue bump, and the strength and shape of the ionizing spectrum. The UV bandpass, unfortunately, is strongly affected by dust extinction. Although the effects of extinction can, in principle, be corrected, in practice such a procedure is fraught with a number of uncertainties, which I briefly mention here.

First, it is unclear how to measure the amount of dust affecting the UV continuum source. Two measures of extinction are traditionally used. One is based on comparison of the observed ratio of a pair of emission lines with their intrinsic ratio, after adopting a form for the extinction law. The intrinsic spectrum of the hydrogen recombination lines is well known for conditions prevailing in the low-density narrow-line regions of AGNs, and the derived optical extinction does not depend sensitively on the exact form of the extinction law. A second method uses the neutral hydrogen column density derived from X-ray spectra to calculate the absorbing column under the assumption that the dust-to-gas ratio and the grain properties are the same as those in the Galaxy. The latter assumptions, however, need not hold, especially in the vicinity of an AGN where grains can be destroyed by the harsh radiation field (Voit 1991). Low values of N_{H} derived from X-ray observations also do not necessarily imply low extinction because some dust can be associated with the ionized medium. In either case, a major source of uncertainty is whether the UV continuum source traverses through the same absorbing medium as probed by the X-rays or by the optical emission lines. The extinction obtained from the X-ray absorbing column in AGN spectra, for instance, often greatly exceeds the extinction inferred from the Balmer decrement (e.g., Reichert et al. 1985).

One can attempt to estimate directly the extinction of the continuum by searching for spectral signatures imprinted by the assumed extinction law. For a Galactic extinction law, the most noticeable feature in the mid-UV is a broad depression centered near 2200 Å. The UV spectra of AGNs, on the other hand, usually do not show this feature (McKee & Petrosian 1974; Neugebauer et al. 1980; Malkan & Oke 1983; Tripp, Bechtold, & Green 1994) despite independent evidence for dust from other indicators (e.g., emission-line ratios). This result implies one or more of the following possibilities: (1) the UV continuum and the line-emitting gas experience different amounts of extinction because the distribution of dust along the line-of-sight is patchy; (2) the strong radiation field destroys dust grains close to the central continuum source; and (3) the extinction law in extragalactic environments differs from that of the Galaxy, specifically in having a much weaker 2200-Å bump. Support for the latter possibility comes from observations of starburst galaxies (Calzetti, Kinney, & Storchi-Bergmann 1994) and of the Small Magellanic Cloud (SMC; Bouchet et al. 1985) whose UV spectra generally show a very weak, if any, 2200-Å bump. Gordon, Calzetti, & Witt (1997) argue that the absence of the 2200-Å feature in these systems is inherent in their extinction law and not merely a consequence of geometry effects. The properties of dust grains, specifically the small graphite grains responsible for the 2200-Å

bump (Mathis 1994), evidently can be greatly affected by environmental conditions such as star-formation activity and/or metallicity. It is not difficult to imagine that the same may be the case in the vicinity of an AGN, where the extinction law can be modified dramatically by the intense radiation field (Laor & Draine 1993; Czerny et al. 1995).

Is the apparent faintness of the UV band intrinsic to the SEDs or is it instead simply a consequence of dust extinction? Luminous AGNs have an optical-UV slope of $\alpha_{\text{ou}} \approx 0.5\text{--}1.0$, whereas in the present sample $\alpha_{\text{ou}} \approx 1.5\text{--}2.0$. Let us estimate how much UV extinction is required to redden the “typical” AGN spectrum to that seen here. Following Maoz et al. (1998), I consider the extinction curve of the SMC (Bouchet et al. 1985), as parameterized by Pei (1992), and the empirical starburst “attenuation curve” of Calzetti et al. (1994), as parameterized by Calzetti (1997). Both curves lack a 2200-Å bump, but the Calzetti et al. curve is greyer. Adopting a fiducial optical and UV wavelength of 6500 Å and 2500 Å, respectively, reddening α_{ou} by a slope of 1 requires $A_V = 0.6$ mag and $A_{2500} = 1.5$ mag for the SMC curve. The shallower Calzetti et al. curve gives $A_V = 1.1$ mag and $A_{2500} = 2.0$ mag. For a more extreme case of $\Delta\alpha_{\text{ou}} = 2$, $A_V = 1.3$ mag and $A_{2500} = 3.0$ mag for the SMC curve, and $A_V = 2.3$ mag and $A_{2500} = 4.1$ mag for the Calzetti et al. curve. These cases are illustrated in Figure 9. Given the limited accuracy of the available data and the unknown form of the extinction law in AGNs, it is difficult to rule out dust reddening as the principal cause of the observed weakness of the UV band, although one can probably exclude Galactic-type dust grains from the absence of the predicted strong 2200-Å feature (thin solid lines in Fig. 9). In fact, the necessary amount of visual extinction, $A_V \approx 1\text{--}2$ mag, is not unreasonable compared to those obtained from the Balmer decrements (Table 1). Note that an average correction of $A_{2500} = 2.0$ mag will change α_{ox} from 0.9 to 1.2, as seen in luminous Seyfert 1s.

Nonetheless, in order to account for the *systematic* differences between the SEDs of the two luminosity classes, one would have to postulate that low-luminosity AGNs *systematically* have either greater levels of extinction or a different dust extinction law compared to high-luminosity AGNs. The first explanation is not supported by the data, at least insofar as Balmer decrements can be used to gauge the continuum extinction; the internal extinctions listed in Table 1 do not appear anomalous compared to those found in more luminous Seyfert galaxies (e.g., Shuder & Osterbrock 1981; Dahari & De Robertis 1988). The second hypothesis is ad hoc and difficult to test experimentally. Moreover, if exposure to the AGN environment indeed does modify the extinction law, one would naïvely expect the effect to be greatest on the most powerful AGNs, exactly the opposite of what is observed. Thus, although dust extinction can in principle be responsible for the spectral peculiarities seen in low-luminosity objects, the alternative view that the nonstandard SEDs are intrinsic to the sources is also tenable and probably more favorable.

5. Summary

Broad-band spectra are presented for seven low-luminosity AGNs. Although the sample is still limited and heterogeneous, this is the most extensive effort so far to systematically investigate the SEDs of these weak sources. Contamination by emission from the host galaxy can severely corrupt the faint signal from the nucleus, and careful attention has been paid to select only the highest quality nuclear fluxes in assembling the SEDs. A comparative study of the gross features of the SEDs reveals that the SEDs of low-luminosity AGNs, as a group, look strikingly different compared to the standard energy spectrum of luminous Seyfert galaxies and QSOs. Most of the differences stem from the exceptional faintness of the UV continuum in the low-luminosity objects. The so-called big blue bump is very weak or altogether absent, thereby making the continuum shape between optical and UV wavelengths steeper than normal and the X-ray band energetically more important. Extinction by dust grains with properties different from those of Galactic composition may be responsible for suppressing the UV emission in low-luminosity AGNs, but an alternative, more intriguing possibility is that the absence of the big blue bump is a property intrinsic to these sources. Another notable property of the SEDs is the prominence of the compact, flat-spectrum radio component relative to the emission in other energy bands. All seven nuclei in the sample, including the three hosted by spiral galaxies, can be considered “radio-loud.” The AGNs investigated here indeed are very quiescent objects. Their bolometric luminosities range from 2×10^{41} to 8×10^{42} ergs s^{-1} , which correspond to an Eddington ratio of $\sim 10^{-6} - 10^{-3}$.

L. C. H. acknowledges financial support from a Harvard-Smithsonian Center for Astrophysics postdoctoral fellowship, from NASA grant NAG 5-3556, and from NASA grants GO-06837.01-95A and AR-07527.02-96A from the Space Telescope Science Institute (operated by AURA, Inc., under NASA contract NAS5-26555). I thank Chien Peng and Edward Moran for assistance in analyzing some of the *HST* and *ROSAT* HRI images, respectively, and I am grateful to Marianne Vestergaard for valuable comments on an earlier version of the paper. I thank Ramesh Narayan for discussions on the theoretical interpretation of the data. This work made extensive use of the NASA/IPAC Extragalactic Database (NED) which is operated by the Jet Propulsion Laboratory, California Institute of Technology, under contract with NASA.

References

- Bääth, L. B., et al. 1992, *A&A*, 257, 31
- Bartel, N., et al. 1982, *ApJ*, 262, 556
- Barth, A. J., Ho, L. C., Filippenko, A. V., & Sargent, W. L. W. 1998, *ApJ*, 496, 133
- Barth, A. J., Reichert, G. A., Filippenko, A. V., Ho, L. C., Shields, J. C., Mushotzky, R. F., & Puchnarewicz, E. M. 1996, *AJ*, 112, 1829
- Bash, F. N., & Kaufman, M. 1986, *ApJ*, 310, 621
- Biretta, J., Stern, C. P., & Harris, D. E. 1991, *AJ*, 101, 1632
- Birkinshaw, M., & Worrall, D. M. 1993, *ApJ*, 412, 568
- Blandford, R. D., & Rees, M. J. 1992, in *Testing the AGN Paradigm*, ed. S. Holt, S. Neff, & M. Urry (New York: AIP), 3
- Bohlin, R. C., Savage, B. D., & Drake, J. K. 1978, *ApJ*, 224, 132
- Bouchet, P., Lequeux, J., Maurice, E., Prevot, L., & Prevot-Burnichon, M. L. 1985, *A&A*, 149, 330
- Bower, G. A., et al. 1998, *ApJ*, 492, L111
- Bower, G. A., Heckman, T. M., Wilson, A. S., & Richstone, D. O. 1997, *ApJ*, 483, L33
- Bower, G. A., Wilson, A. S., Heckman, T. M., & Richstone, D. O. 1996, *AJ*, 111, 1901
- Calzetti, D. 1997, in *The Ultraviolet Universe at Low and High Redshift*, ed. W. H. Waller et al. (New York: AIP), 403
- Calzetti, D., Kinney, A. L., & Storchi-Bergmann, T. 1994, *ApJ*, 429, 582
- Cardelli, J. A., Clayton, G. C., & Mathis, J. S. 1989, *ApJ*, 345, 245
- Cohen, M. H., & Readhead, A. C. S. 1979, *ApJ*, 233, L101
- Crane, P., et al. 1993, *AJ*, 106, 1371
- Crane, P., & Vernet, J. 1997, *ApJ*, 486, L91
- Czerby, B., Loska, Z., Szczerba, R., Cukierska, J., & Madejski, G. 1995, *AcA*, 45, 623
- Dahari, O., & De Robertis, M. M. 1988, *ApJS*, 67, 249
- de Vaucouleurs, G., de Vaucouleurs, A., Corwin, H. G., Jr., Buta, R. J., Paturel, G., & Fouqué, R. 1991, *Third Reference Catalogue of Bright Galaxies* (New York: Springer)
- Devereux, N. A., Becklin, E. E., & Scoville, N. 1987, *ApJ*, 312, 529
- Devereux, N. A., Ford, H. C., & Jacoby, G. 1997, *ApJ*, 481, L71
- Elvis, M., et al. 1994, *ApJS*, 95, 1
- Fabbiano, G., Fassnacht, C., & Trinchieri, G. 1994, *ApJ*, 434, 67
- Fabbiano, G., & Juda, J. Z. 1997, *ApJ*, 476, 666
- Fabbiano, G., Kim, D.-W., & Trinchieri, G. 1992, *ApJS*, 80, 531
- Fabian, A. C., Rees, M. J., Stella, L., & White, N. E. 1989, *MNRAS*, 238, 729
- Ferrarese, L., Ford, H. C., & Jaffe, W. 1996, *ApJ*, 470, 444

- Forbes, D. A., Ward, M. J., DePoy, D. L., Boisson, C., & Smith, M. S. 1992, *MNRAS*, 254, 509
- Gaskell, C. M., & Ferland, G. J. 1984, *PASP*, 96, 393
- González-Delgado, R. M., & Pérez, E. 1996, *MNRAS*, 281, 1105
- Gordon, K. D., Calzetti, D., & Witt, A. N. 1997, *ApJ*, 487
- Heckman, T. M. 1980, *A&A*, 87, 152
- Ho, L. C. 1998c, in *Observational Evidence for Black Holes in the Universe*, ed. S. K. Chakrabarti (Dordrecht: Kluwer), 157
- Ho, L. C. 1999a, in *The AGN-Galaxy Connection*, ed. H. R. Schmitt, L. C. Ho, & A. L. Kinney (Advances in Space Research), in press
- Ho, L. C. 1999b, in preparation
- Ho, L. C., et al. 1999b, in preparation
- Ho, L. C., Filippenko, A. V., & Sargent, W. L. W. 1995, *ApJS*, 98, 477
- Ho, L. C., Filippenko, A. V., & Sargent, W. L. W. 1996, *ApJ*, 462, 183
- Ho, L. C., Filippenko, A. V., & Sargent, W. L. W. 1997a, *ApJ*, 487, 568
- Ho, L. C., Filippenko, A. V., & Sargent, W. L. W. 1997b, *ApJS*, 112, 315
- Ho, L. C., Van Dyk, S. D., Pooley, G. G., Sramek, R. A., & Weiler, K. W. 1999a, *AJ*, submitted
- Hummel, E., van der Hulst, J. M., & Dickey, J. M. 1984, *A&A*, 134, 207
- Impey, C. D., Wynn-Williams, C. G., & Becklin, E. E. 1986, *ApJ*, 309, 572
- Ishisaki, Y., et al. 1996, *PASJ*, 48, 237
- Jones, D. L., et al. 1986, *ApJ*, 305, 684
- Jones, D. L., Terzian, Y., & Sramek, R. A. 1981, *ApJ*, 246, 28
- Jones, D. L., & Wehrle, A. E. 1997, *ApJ*, 484, 186
- Kellermann, K. I., Sramek, R. A., Schmidt, M., Shaffer, D. B., & Green, R. F. 1989, *AJ*, 98, 1195
- Kormendy, J., et al. 1997, *ApJ*, 473, L91
- Laor, A., & Draine, B. 1993, *ApJ*, 402, 441
- Lasota, J.-P., Abramowicz, M. A., Chen, X., Krolik, J., Narayan, R., & Yi, I. 1996, *ApJ*, 462, 142
- Maiolino, R., Ruiz, M., Rieke, G. H., & Keller, L. D. 1995, *ApJ*, 446, 561
- Malkan, M. A., & Oke, J. B. 1983, *ApJ*, 265, 92
- Malkan, M. A., & Sargent, W. L. W. 1982, *ApJ*, 254, 22
- Maoz, D., Filippenko, A. V., Ho, L. C., Rix, H.-W., Bahcall, J. N., Schneider, D. P., & Macchetto, F. D. 1995, *ApJ*, 440, 91
- Maoz, D., Koratkar, A. P., Shields, J. C., Ho, L. C., Filippenko, A. V., & Sternberg, A. 1998, *AJ*, 116, 55
- Mathis, J. S. 1994, *ApJ*, 422, 176
- McKee, C. F., & Petrosian, V. 1974, *ApJ*, 189, 17
- Murphy, E. M., Lockman, F. J., Laor, A., & Elvis, M. 1996, *ApJS*, 105, 369

- Mushotzky, R. F., & Wandel, A. 1989, *ApJ*, 339, 674
- Nandra, K., George, I. M., Mushotzky, R. F., Turner, T. J., & Yaqoob, T. 1997, *ApJ*, 477, 602
- Neugebauer, G., et al. 1980, *ApJ*, 238, 502
- Nicholson, K. L., Reichert, G. A., Mason, K. O., Puchnarewicz, E. M., Ho, L. C., Shields, J. C., & Filippenko, A. V. 1998, *MNRAS*, 300, 893
- Pauliny-Toth, I. I. K., Preuss, E., Witzel, A., Graham, D., Kellermann, K. I., Ronnang, B. 1981, *AJ*, 86, 371
- Pei, Y. C. 1992, *ApJ*, 395, 130
- Reichert, G. A., Mushotzky, R. F., Petre, R., & Holt, S. S. 1985, *ApJ*, 296, 69
- Reid, M. J., Biretta, J. A., Junor, W., Muxlow, T. W. B., & Spencer, R. E. 1989, *ApJ*, 336, 112
- Reynolds, C. S., Di Matteo, T., Fabian, A. C., Hwang, U., & Canizares, C. R. 1996, *MNRAS*, 283, L111
- Rieke, G. H., & Lebofsky, M. J. 1978, *ApJ*, 220, L37
- Sadler, E. M., Slee, O. B., Reynolds, J. E., & Roy, A. L. 1995, *MNRAS*, 276, 1373
- Sanders, D. B., Phinney, E. S., Neugebauer, G., Soifer, B. T., & Matthews, K. 1989, *ApJ*, 347, 29
- Schilizzi, R. T. 1976, *AJ*, 81, 946
- Serlemitsos, P., Ptak, A., & Yaqoob, T. 1996, in *The Physics of LINERs in View of Recent Observations*, ed. M. Eracleous et al. (San Francisco: ASP), 70
- Shields, G. A. 1978, *Nature*, 272, 706
- Shuder, J. M., & Osterbrock, D. E. 1981, *ApJ*, 250, 55
- Soltan, A. 1982, *MNRAS*, 200, 115
- Spencer, R. E., & Junor, W. 1986, *Nature*, 321, 753
- Stiavelli, M., Peletier, R. F., & Carollo, C. M. 1997, *MNRAS*, 285, 181
- Terashima, Y., Kunieda, H., Misaki, K., Mushotzky, R. F., Ptak, A. F., & Reichert, G. A. 1998, *ApJ*, 503, 212
- Tripp, T. M., Bechtold, J., Green, R. F. 1994, *ApJ*, 433, 533
- Tsvetanov, Z. I., Hartig, G. F., Ford, H. C., Kriss, G. A., Dopita, M. A., Dressel, L. L., & Harms, R. J. 1998, in *Proceedings of the M87 Workshop (Lecture Notes in Physics: Springer Verlag)*, in press
- Turner, J. L., & Ho, P. T. P. 1994, *ApJ*, 421, 122
- Turner, T. J., George, I. M., Nandra, K., & Mushotzky, R. F. 1997, *ApJS*, 113, 23
- Turner, T. J., & Pounds, K. A. 1989, *MNRAS*, 240, 833
- Voit, G. M. 1991, *ApJ*, 379, 122
- Willner, S. P., Elvis, M., Fabbiano, G., Lawrence, A., & Ward, M. J. 1985, *ApJ*, 299, 443
- Worrall, D. M., & Birkinshaw, M. 1994, *ApJ*, 427, 134
- Zirbel, E. L., & Baum, S. A. 1998, *ApJS*, 114, 177

TABLE 1
PROPERTIES OF THE SAMPLE

Object Name (1)	Hubble Type (2)	AGN Class (3)	D (Mpc) (4)	M_{BT}^0 (mag) (5)	M_{BH} (M_{\odot}) (6)	A_V (Gal) (mag) (7)	A_V (int) (mag) (8)	Ref. (9)
NGC 3031 (M81)	Sab	S1.5/L1.5	3.6	-20.39	4×10^6	0.12	0.17 (0.53)	1 (2)
NGC 4261 (3C 270)	E2	L2	30.0	-21.37	4.9×10^8	0.09	1.4 (<0.2)	3 (4)
NGC 4374 (M84)	E1	L2	16.8	-21.12	1.5×10^9	0.09	1.3	3
NGC 4486 (M87)	E0	L2	16.8	-21.67	3×10^9	0.08	1.0	3
NGC 4579 (M58)	SABb	S1.9/L1.9	16.8	-20.84	4×10^6	0.16	2.1 (0.21)	5 (6)
NGC 4594 (M104)	Sa	L2	9.2	-21.44	1×10^9	0.20	0.25 (0.28)	3 (7)
NGC 6251	E0	S2	92.0	-21.59	7.5×10^8	0.30	5.0 (0.75)	8 (9)

NOTE.— Cols.: (1) Galaxy name; (2) Hubble type, from de Vaucouleurs et al. 1991; (3) spectral classification of the nucleus from Ho et al. 1997b (except for NGC 6251, which comes from Shuder & Osterbrock 1981), where L = LINER and S = Seyfert; type 2 objects have no detectable broad lines, type 1.9 objects exhibit broad $H\alpha$, and type 1.5 implies fairly prominent broad $H\alpha$ and $H\beta$; (4) distance adopted; (5) total absolute blue magnitude corrected for Galactic and internal extinction, with apparent magnitudes taken from de Vaucouleurs et al. 1991 and distances from column 4; (6) mass of the central black hole taken from the compilation of Ho 1998, except for NGC 4579, which comes from Barth et al. 1996; (7) Galactic extinction taken from de Vaucouleurs et al. 1991 (M81, NGC 4261, M84, and M87) or derived based on H I column densities N_H from Murphy et al. 1996 and the conversions $E(B - V) = N_H / (5.8 \times 10^{21} \text{ cm}^{-2})$ mag and $A_V / E(B - V) = 3.1$ (NGC 4579, 4594, and 6251); (8) internal extinction derived from the Balmer decrement and, in parentheses, from the X-ray absorbing column; (9) reference for the Balmer decrement, and, in parentheses, for the X-ray absorbing column.

REFERENCES.— (1) Ho et al. 1996; (2) Ishizaki et al. 1996; (3) Ho et al. 1997b; (4) Worrall & Birkinshaw 1994; (5) González-Delgado & Pérez 1996; (6) Terashima et al. 1998; (7) Nicholson et al. 1998; (8) Shuder & Osterbrock 1981; (9) Turner et al. 1997.

TABLE 2
DATA FOR THE NUCLEUS OF M81

ν (Hz)	νF_ν (ergs s ⁻¹ cm ⁻²)	Resolution ($''$)	Reference
1.41×10^9	7.59×10^{-16}	1	Bash& Kaufman (1986)
1.49×10^9	6.76×10^{-16}	1	Turner & Ho (1994)
2.29×10^9	1.45×10^{-15}	0.001	Bartel et al. (1982)
4.85×10^9	4.47×10^{-15}	1	Turner & Ho (1994)
8.32×10^9	6.03×10^{-15}	0.001	Bartel et al. (1982)
1.50×10^{10}	1.35×10^{-14}	0.2	Ho et al. (1998) ^a
3.02×10^{13}	$< 2.24 \times 10^{-11}$	3.9	Rieke & Lebofsky (1978)
8.57×10^{13}	$< 3.80 \times 10^{-11}$	3	Forbes et al. (1992)
1.36×10^{14}	$< 1.02 \times 10^{-10}$	3	Forbes et al. (1992)
1.81×10^{14}	$< 1.48 \times 10^{-10}$	3	Forbes et al. (1992)
2.50×10^{14}	$< 1.69 \times 10^{-10}$	3	Forbes et al. (1992)
4.95×10^{14}	1.53×10^{-11}	0.2	Bower et al. (1996) ^b
6.25×10^{14}	1.22×10^{-11}	0.1	Devereux et al. (1997) ^b
6.27×10^{14}	1.39×10^{-11}	0.3	Ho et al. (1996) ^c
1.35×10^{15}	4.07×10^{-11}	0.3	Ho et al. (1996) ^c
1.87×10^{15}	2.38×10^{-12}	0.3	Ho et al. (1996) ^d
2.00×10^{15}	9.09×10^{-12}	0.1	Devereux et al. (1997) ^b
2.60×10^{15}	1.61×10^{-12}	0.3	Ho et al. (1996) ^d
4.84×10^{17}	6.60×10^{-12}	300	Ishisaki et al. (1996) ^e
2.42×10^{18}	8.38×10^{-12}	300	Ishisaki et al. (1996) ^e

^aAverage flux density excluding the outburst phases.

^bDereddened by $E(B - V) = 0.094$ mag following Ho et al. 1996.

^cContinuous *HST* spectrum from 6.3×10^{14} Hz to 1.4×10^{15} Hz.

^dContinuous *HST* spectrum from 1.9×10^{15} Hz to 2.6×10^{15} Hz.

^eContinuous *ASCA* spectrum from 2–10 keV.

TABLE 3
DATA FOR THE NUCLEUS OF NGC 4261

ν (Hz)	νF_ν (ergs s ⁻¹ cm ⁻²)	Resolution ($''$)	Reference
1.63×10^9	1.63×10^{-15}	0.012	Jones & Wehrle (1997)
8.39×10^9	8.39×10^{-15}	0.0012	Jones & Wehrle (1997)
3.00×10^{13}	$< 8.97 \times 10^{-12}$	5.7	Impey et al. (1986)
7.89×10^{13}	$< 2.53 \times 10^{-11}$	5.8	Impey et al. (1986)
1.36×10^{14}	$< 8.46 \times 10^{-11}$	5.8	Impey et al. (1986)
1.82×10^{14}	$< 1.44 \times 10^{-10}$	5.8	Impey et al. (1986)
2.40×10^{14}	$< 1.48 \times 10^{-10}$	7.5	Impey et al. (1986)
3.64×10^{14}	4.09×10^{-14}	0.1	Ferrarese et al. (1996) ^a
4.41×10^{14}	3.12×10^{-14}	0.1	Ferrarese et al. (1996) ^a
5.41×10^{14}	2.69×10^{-14}	0.1	Ferrarese et al. (1996) ^a
1.30×10^{15}	$< 1.38 \times 10^{-16}$	0.1	Zirbel & Baum (1998) ^a
2.42×10^{17}	2.71×10^{-13}	25	Worral & Birkinshaw (1994) ^b

^aDereddened by $A_V = 0.084$ mag.

^bSpatially unresolved, power-law component derived from fitting the *ROSAT* PSPC data. Worral & Birkinshaw 1994 find that at least 50% of the total PSPC flux comes from the unresolved component.

TABLE 4
DATA FOR THE NUCLEUS OF M84

ν (Hz)	νF_ν (ergs s ⁻¹ cm ⁻²)	Resolution ($''$)	Reference
1.67×10^9	2.67×10^{-15}	0.004	Jones et al. (1981)
8.09×10^9	1.54×10^{-14}	0.03	Schilizzi (1976)
3.00×10^{13}	$< 6.30 \times 10^{-12}$	5.5	Devereux et al. (1987)
1.36×10^{14}	$< 1.29 \times 10^{-10}$	5.5	Devereux et al. (1987)
1.82×10^{14}	$< 2.29 \times 10^{-10}$	5.5	Devereux et al. (1987)
2.40×10^{14}	$< 2.23 \times 10^{-10}$	5.5	Devereux et al. (1987)
3.63×10^{14}	2.46×10^{-12}	0.1	Bower et al. (1997) ^a
5.50×10^{14}	1.00×10^{-12}	0.1	Bower et al. (1997) ^a
1.30×10^{15}	$< 4.52 \times 10^{-15}$	0.1	Zirbel & Baum (1998) ^a
4.84×10^{17}	$< 8.90 \times 10^{-13}$	4	Fabbiano et al. (1992)

^aAdopting $A_V = 1.39$ mag (0.099 mag Galactic, 1.3 mag internal; see text).

TABLE 5
DATA FOR THE NUCLEUS OF M87

ν (Hz)	νF_ν (ergs s ⁻¹ cm ⁻²)	Resolution ($''$)	Reference
1.47×10^9	$< 5.39 \times 10^{-14}$	1.2	Biretta et al. (1991)
1.66×10^9	1.65×10^{-14}	0.005	Reid et al. (1989)
4.89×10^9	$< 1.66 \times 10^{-13}$	1.2	Biretta et al. (1991)
5.00×10^9	1.00×10^{-14}	0.0007	Pauliny-Toth et al. (1981)
1.49×10^{10}	$< 4.43 \times 10^{-13}$	1.2	Biretta et al. (1991)
2.20×10^{10}	4.80×10^{-14}	0.00015	Spencer & Junor (1986)
1.00×10^{11}	8.66×10^{-13}	0.0001	Bääth et al. (1992)
2.97×10^{13}	$< 3.18 \times 10^{-11}$	6	Willner et al. (1985)
1.36×10^{14}	$< 2.96 \times 10^{-12}$	1	Stiavelli et al. (1997)
2.50×10^{14}	$< 6.13 \times 10^{-12}$	0.9	Stiavelli et al. (1997)
3.63×10^{14}	2.39×10^{-12}	0.1	<i>HST</i> archive ^a
3.82×10^{14}	2.86×10^{-12}	0.1	<i>HST</i> archive ^b
4.41×10^{14}	3.28×10^{-12}	0.2	Tsvetanov et al. (1998) ^c
6.67×10^{14}	2.77×10^{-12}	0.2	Tsvetanov et al. (1998) ^c
1.30×10^{15}	3.04×10^{-12}	0.1	Maoz et al. (1995) ^d
2.50×10^{15}	1.03×10^{-12}	0.2	Tsvetanov et al. (1998) ^c
2.42×10^{17}	8.50×10^{-13}	4	Biretta et al. (1991)
2.42×10^{17}	1.60×10^{-12}	4	Reynolds et al. (1996)
4.84×10^{17}	$< 7.00 \times 10^{-12}$	200	Reynolds et al. (1996)

^aImage taken with WFPC2 in the F814W filter; dereddened by $A_V = 0.12$ mag.

^bImage taken with WFPC1 in the F785LP filter; dereddened by $A_V = 0.12$ mag.

^cContinuous *HST* spectrum from 4.4×10^{14} Hz to 2.5×10^{15} Hz.

^dDereddened by $A_V = 0.12$ mag.

TABLE 6
DATA FOR THE NUCLEUS OF NGC 4579

ν (Hz)	νF_ν (ergs s ⁻¹ cm ⁻²)	Resolution ($''$)	Reference
2.30×10^9	4.78×10^{-16}	0.03	Sadler et al. (1995)
8.40×10^9	2.24×10^{-15}	0.03	Sadler et al. (1995)
1.49×10^{13}	$< 8.32 \times 10^{-12}$	6	Willner et al. (1985)
2.97×10^{13}	$< 1.99 \times 10^{-11}$	6	Willner et al. (1985)
6.25×10^{13}	$< 1.48 \times 10^{-11}$	6	Willner et al. (1985)
8.57×10^{13}	$< 4.07 \times 10^{-11}$	6	Willner et al. (1985)
1.36×10^{14}	$< 1.02 \times 10^{-10}$	6	Willner et al. (1985)
1.81×10^{14}	$< 1.66 \times 10^{-10}$	6	Willner et al. (1985)
2.50×10^{14}	$< 1.74 \times 10^{-10}$	6	Willner et al. (1985)
6.67×10^{14}	7.59×10^{-13}	0.43	Barth et al. (1996) ^a
9.15×10^{14}	1.30×10^{-12}	0.43	Barth et al. (1996) ^b
1.30×10^{15}	2.26×10^{-12}	0.1	Maoz et al. (1996)
2.59×10^{15}	5.51×10^{-13}	0.43	Barth et al. (1996) ^b
4.84×10^{17}	2.04×10^{-12}	300	Terashima et al. (1998) ^c
2.42×10^{18}	3.19×10^{-12}	300	Terashima et al. (1998) ^c

^aExtrapolated from the *HST* UV continuum based on $F_\nu \propto \nu^{-1.0}$.

^bContinuous *HST* spectrum from 9.2×10^{14} Hz to 2.6×10^{15} Hz.

^cContinuous *ASCA* spectrum from 2–10 keV.

TABLE 7
DATA FOR THE NUCLEUS OF NGC 4594

ν (Hz)	νF_ν (ergs s ⁻¹ cm ⁻²)	Resolution ($''$)	Reference
6.10×10^8	3.42×10^{-16}	<1	Hummel et al. (1984)
1.42×10^9	1.07×10^{-15}	0.01	Hummel et al. (1984)
2.69×10^9	2.74×10^{-15}	<1	Hummel et al. (1984)
4.89×10^9	6.01×10^{-15}	0.5	Hummel et al. (1984)
8.09×10^9	9.14×10^{-15}	0.07	Hummel et al. (1984)
1.50×10^{10}	1.50×10^{-14}	0.2	Hummel et al. (1984)
2.83×10^{13}	$< 8.77 \times 10^{-12}$	5.3	Maiolino et al. (1995)
8.57×10^{13}	$< 5.25 \times 10^{-11}$	5	Willner et al. (1985)
1.36×10^{14}	$< 1.20 \times 10^{-10}$	5	Willner et al. (1985)
1.81×10^{14}	$< 2.39 \times 10^{-11}$	5	Willner et al. (1985)
2.50×10^{14}	$< 2.45 \times 10^{-10}$	5	Willner et al. (1985)
3.63×10^{14}	1.16×10^{-12}	0.1	<i>HST</i> archive ^a
4.41×10^{14}	4.41×10^{-12}	0.2	Kormendy et al. (1997) ^b
5.50×10^{14}	1.02×10^{-12}	0.1	<i>HST</i> archive ^c
6.59×10^{14}	1.61×10^{-12}	0.2	Kormendy et al. (1997) ^b
9.17×10^{14}	1.53×10^{-12}	0.9	Nicholson et al. (1998) ^d
2.50×10^{15}	3.79×10^{-13}	0.9	Nicholson et al. (1998) ^d
2.42×10^{17}	8.42×10^{-13}	4	Fabbiano & Juda (1997)
4.84×10^{17}	1.07×10^{-12}	300	Nicholson et al. (1998) ^e
2.42×10^{18}	1.94×10^{-12}	300	Nicholson et al. (1998) ^e

^aImage taken with WFPC2 in the F814W filter.

^bContinuous *HST* spectrum from 4.4×10^{14} Hz to 6.6×10^{14} Hz. The spectrum was divided by 2 to account for the average contamination from starlight estimated by Kormendy et al. 1997.

^cImage taken with WFPC2 in the F547M filter.

^dContinuous *HST* spectrum from 9.2×10^{14} Hz to 2.5×10^{15} Hz.

^eContinuous *ASCA* spectrum from 2–10 keV.

TABLE 8
DATA FOR THE NUCLEUS OF NGC 6251

ν (Hz)	νF_ν (ergs s ⁻¹ cm ⁻²)	Resolution ($''$)	Reference
1.67×10^9	4.66×10^{-15}	0.0030	Jones et al. (1986)
2.31×10^9	5.71×10^{-15}	0.0021	Jones et al. (1986)
5.00×10^9	1.75×10^{-14}	0.0012	Jones et al. (1986)
1.07×10^{10}	9.63×10^{-14}	0.0006	Cohen & Readhead (1979)
3.69×10^{14}	7.00×10^{-13}	0.1	Crane & Vernet (1997)
5.41×10^{14}	5.55×10^{-13}	0.1	Crane & Vernet (1997)
7.32×10^{14}	$>4.10 \times 10^{-13}$	0.1	Crane & Vernet (1997) ^a
8.82×10^{14}	$>2.48 \times 10^{-13}$	0.1	Crane & Vernet (1997) ^a
2.42×10^{17}	7.45×10^{-13}	25	Worrall & Birkinshaw (1994) ^b
4.84×10^{17}	8.81×10^{-13}	300	Turner et al. (1997) ^c
2.42×10^{18}	7.38×10^{-13}	300	Turner et al. (1997) ^c

^aAccording to Crane & Vernet 1997, the reported flux should be taken as a lower limit because the FOC data were not corrected for the nonlinear behavior of the detector.

^bSpatially unresolved, power-law component derived from fitting the *ROSAT* PSPC data. Birkinshaw & Worrall 1993 find that $\sim 90\%$ of the total PSPC flux comes from an unresolved component with a diameter $\lesssim 4''$.

^cContinuous *ASCA* spectrum from 2–10 keV.

TABLE 9
SPECTRAL CHARACTERISTICS

Object Name (1)	L_{bol} (L_{\odot}) (2)	$L_{\text{bol}}/L_{\text{E}}$ (3)	M_B^{nuc} (mag) (4)	$P_{6\text{cm}}$ (W Hz $^{-1}$) (5)	$L_{\text{x}}(0.5\text{--}10\text{ keV})$ (ergs s $^{-1}$) (6)	α_{ox} (7)	α_{x} (8)	α_{ou} (9)
NGC 3031 (M81)	2.1×10^{41}	4.2×10^{-4}	-11.35	1.4×10^{20}	3.2×10^{40}	1.08	0.85	1.4
NGC 4261 (3C 270)	1.7×10^{42}	2.8×10^{-5}	-8.94	1.1×10^{22}	1.2×10^{41}	0.44–0.84	...	2.1
NGC 4374 (M84)	8.2×10^{41}	4.3×10^{-6}	-11.41	6.1×10^{21}	9.8×10^{40}	0.75	...	3.5
NGC 4486 (M87)	2.3×10^{42}	6.1×10^{-6}	-12.95	6.8×10^{21}	1.3×10^{41}	1.06	...	1.6
NGC 4579 (M58)	9.9×10^{41}	1.9×10^{-3}	-11.55	8.1×10^{20}	3.2×10^{41}	0.78–1.02	0.72	1.0
NGC 4594 (M104)	2.7×10^{41}	2.2×10^{-6}	-10.42	1.2×10^{21}	3.6×10^{40}	0.89	0.63	1.4
NGC 6251	8.0×10^{42}	8.5×10^{-5}	-14.70	3.6×10^{23}	2.7×10^{42}	0.83	1.11	1.7

NOTE.— Cols.: (1) Galaxy name; (2) bolometric luminosity of the nucleus obtained by integrating the interpolated SEDs shown in Figure 8; (3) bolometric luminosity normalized to the Eddington value; (4) absolute B -band magnitude of the nonstellar featureless continuum of the nucleus; (5) radio power of the nucleus at 6 cm; (6) X-ray luminosity from 0.5–10 keV assuming the X-ray continuum slope α_{x} given in column 8; for the three cases where α_{x} is not known (NGC 4261, M84, and M87), $\alpha_{\text{x}} = 0.7$ is adopted; (7) two-point spectral index between 2500 Å and 2 keV, where $F_{\nu} \propto \nu^{-\alpha_{\text{ox}}}$; (8) power-law index of the continuum in the hard X-ray (2–10 keV) band; (9) approximate power-law index of the optical-UV continuum.

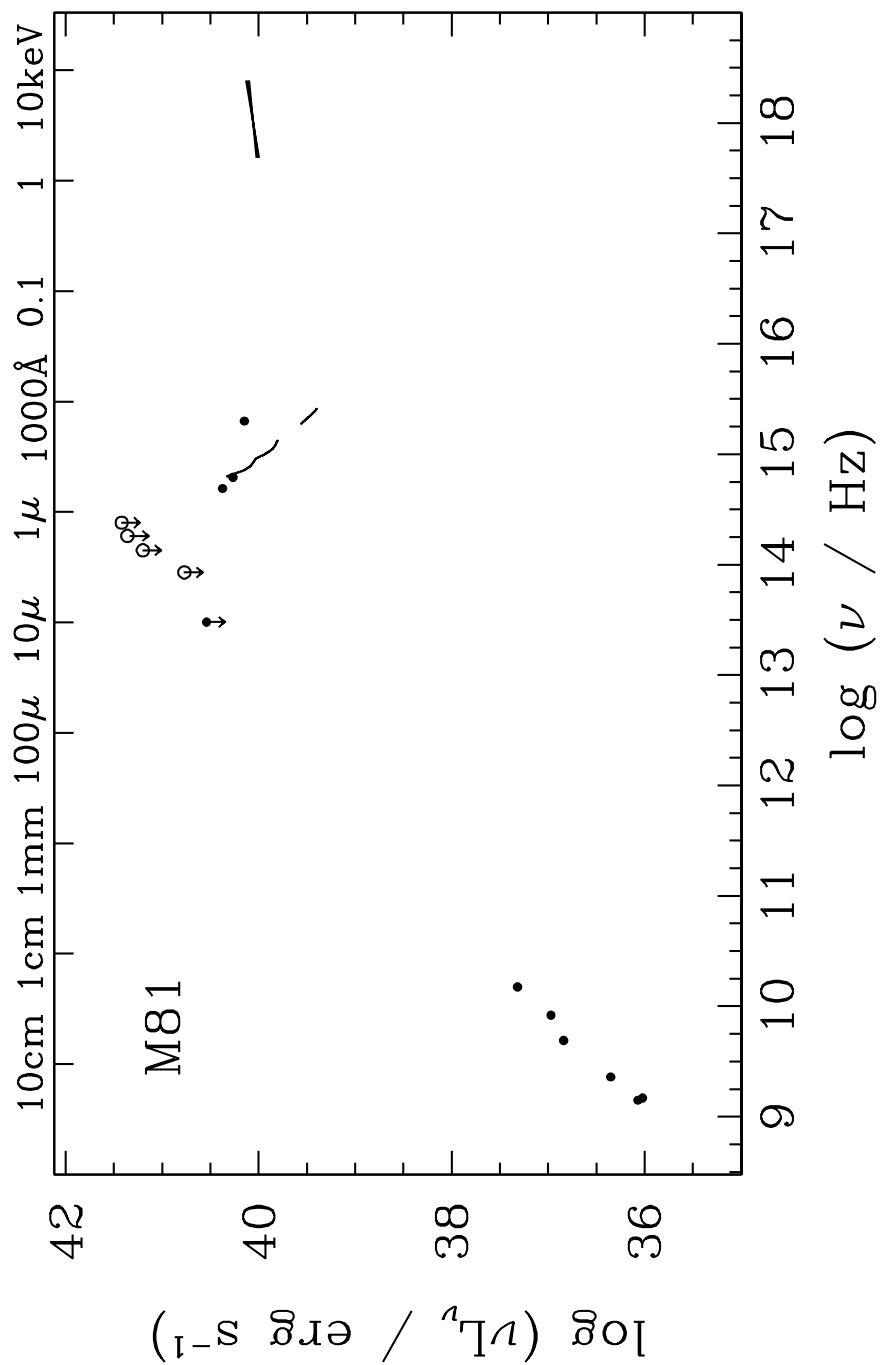


Fig. 1.— Spectral energy distribution of M81 (see Table 2). In this and in subsequent figures, open symbols denote data that are believed to be heavily contaminated by non-nuclear emission.

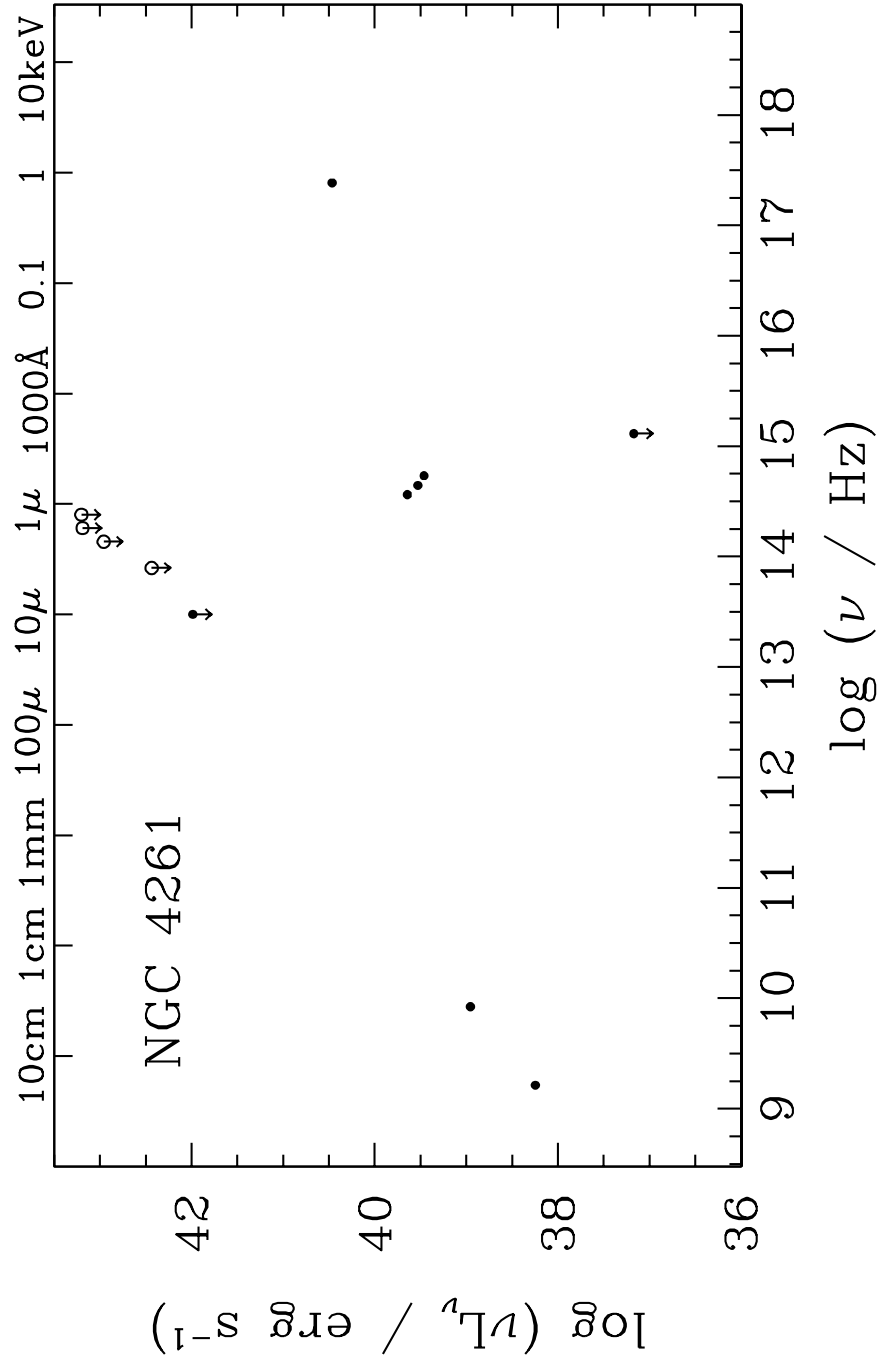


Fig. 2.— Spectral energy distribution of NGC 4261 (see Table 3).

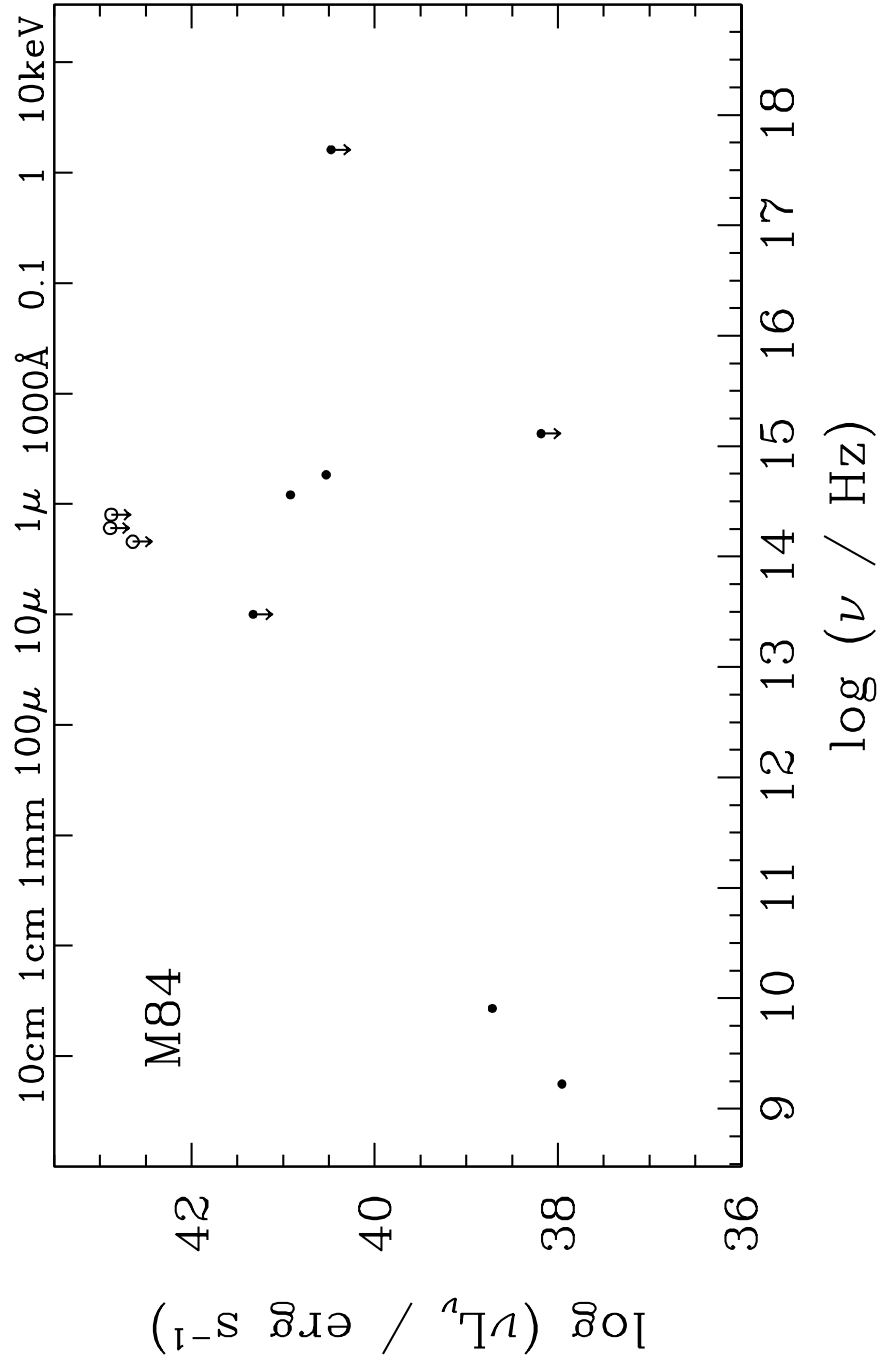


Fig. 3.— Spectral energy distribution of M84 (see Table 4).

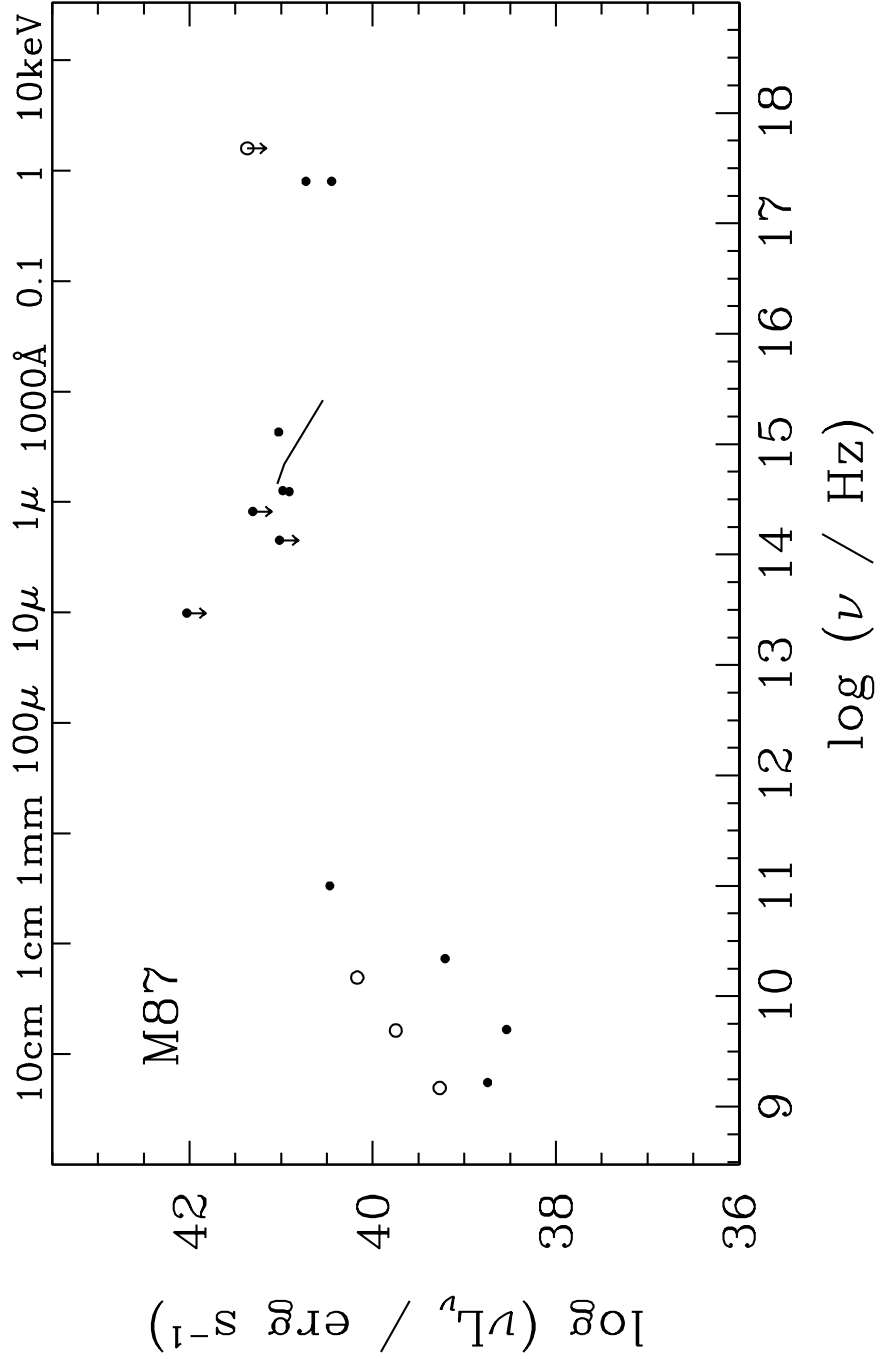


Fig. 4.— Spectral energy distribution of M87 (see Table 5). The three radio points in *open* symbols were obtained with a relatively large beam. They are plotted along with the VLBI points (*solid* symbols) to illustrate the effects of contamination by the radio jet.

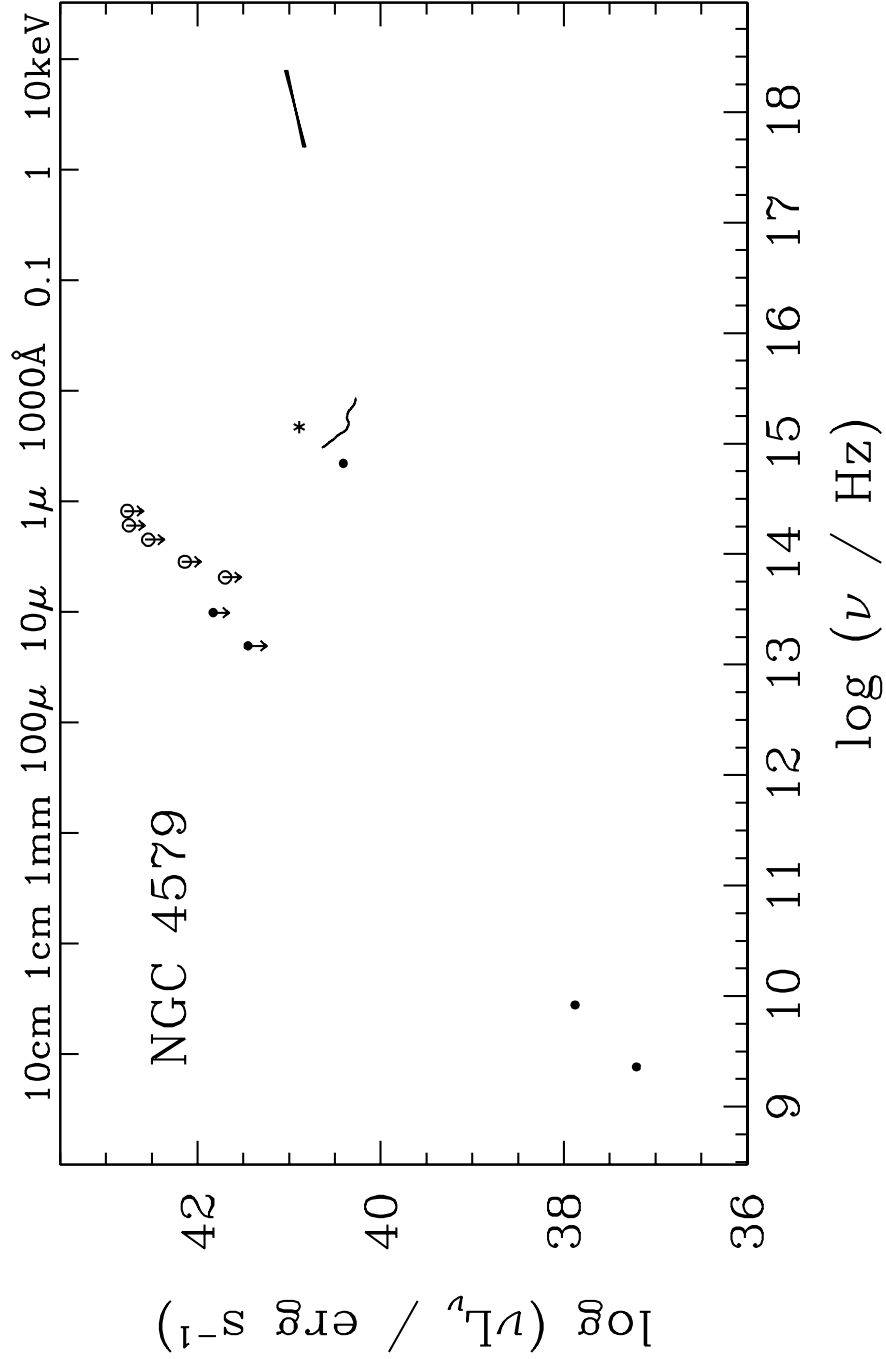


Fig. 5.— Spectral energy distribution of NGC 4579 (see Table 6). The UV point ($\log \nu = 15.1$) measured with the FOC (*asterisk*) is a factor of 3–4 higher than the corresponding flux in the FOS spectrum (*solid line*). Barth et al. (1996) and Maoz et al. (1998) argue that the difference is due to variability.

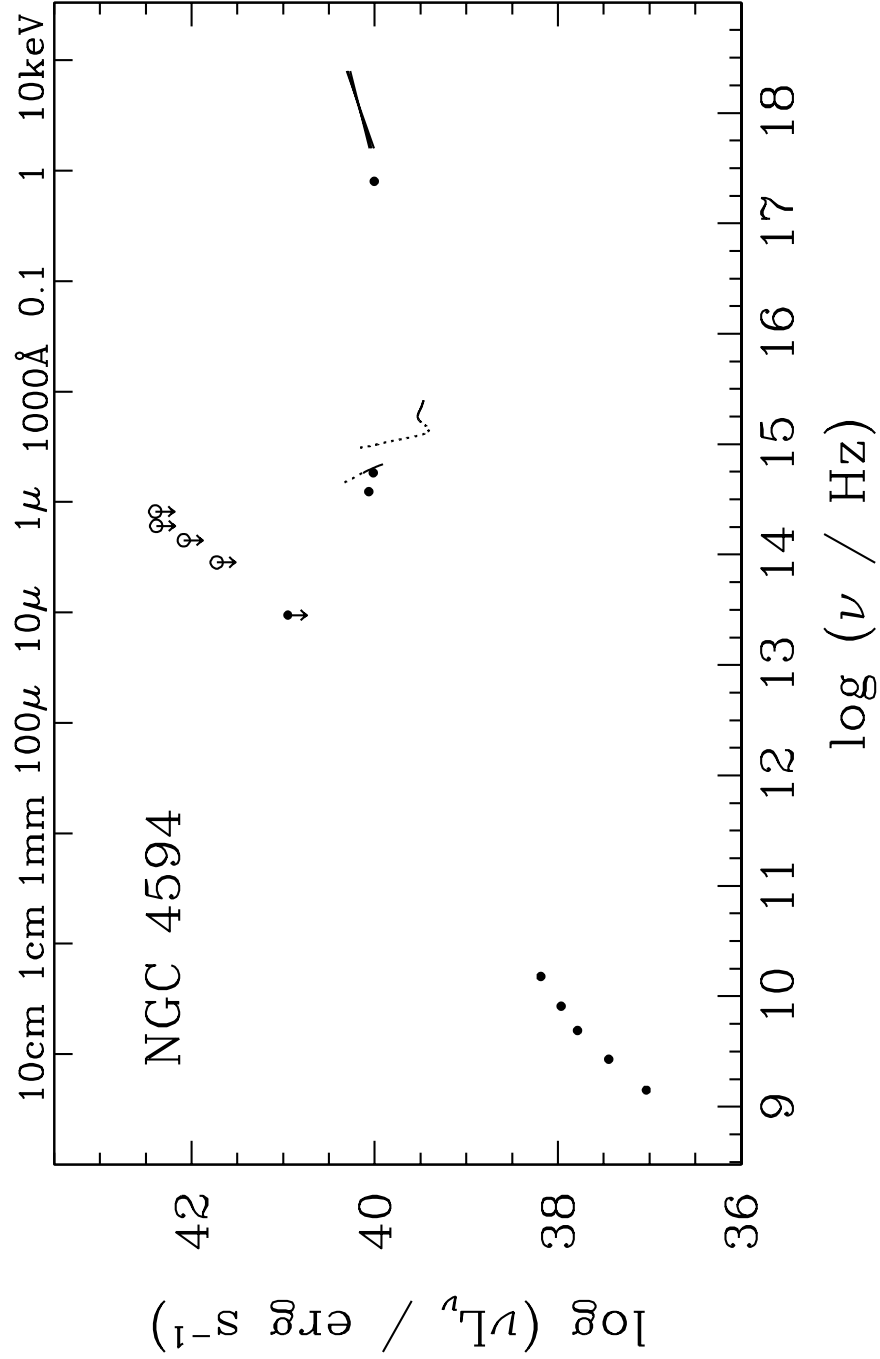


Fig. 6.— Spectral energy distribution of NGC 4594 (see Table 7). The portions of the FOS spectra that are contaminated by starlight are plotted as *dotted lines*.

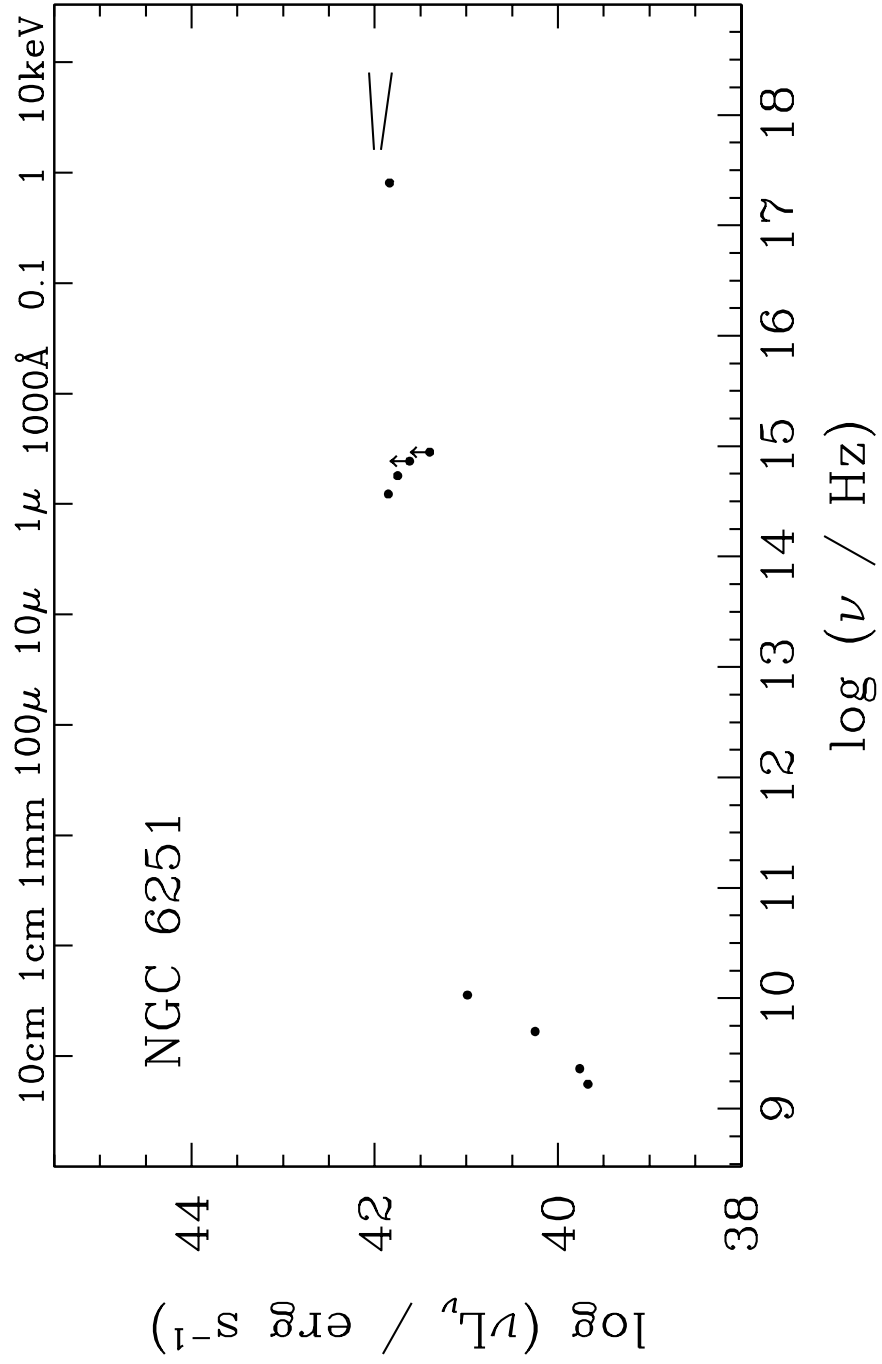


Fig. 7.— Spectral energy distribution of NGC 6251 (see Table 8).

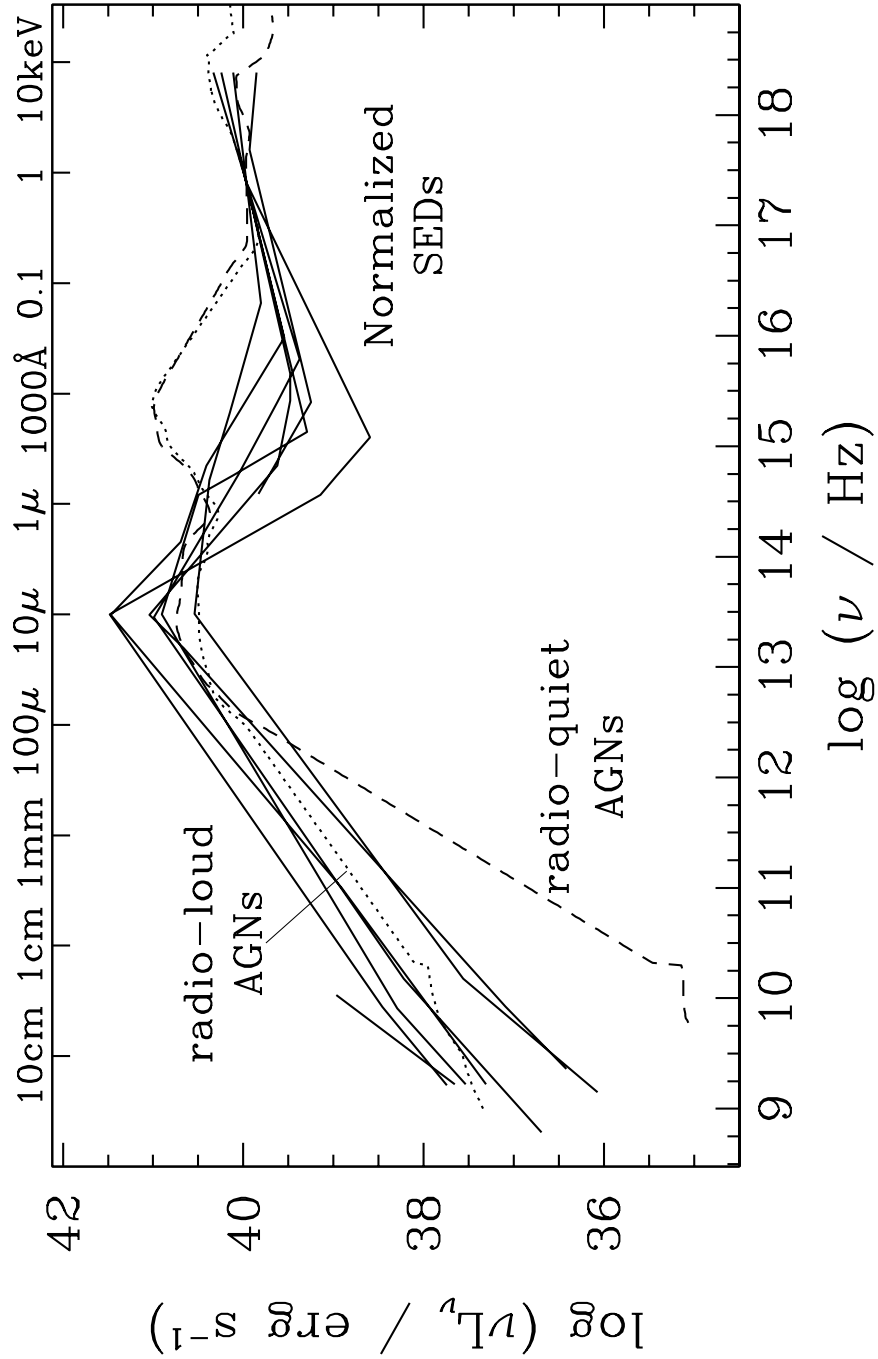


Fig. 8.— Interpolated SEDs of all the objects (*solid lines*) normalized to the 1 keV luminosity of M81. The median radio-loud (*dotted line*) and radio-quiet (*dashed line*) SEDs of Elvis et al. (1994), normalized similarly, are overplotted for comparison.

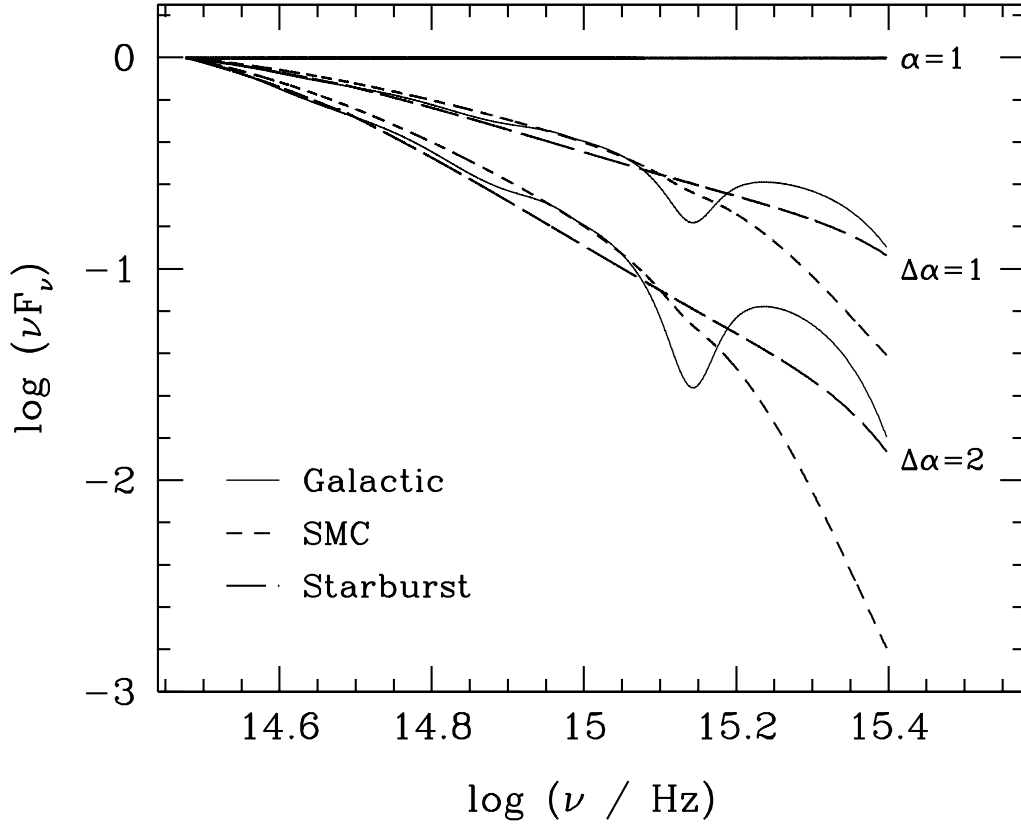


Fig. 9.— The effect of different extinction laws on the SED from 1200 \AA to $1 \mu\text{m}$. The intrinsic (unextincted) continuum is assumed to be a single power law with $\alpha = 1$ (top curve, *heavy solid* line), and it was reddened such that the optical-UV slope between 6500 \AA and 2500 \AA changes by $\Delta\alpha = 1$ (middle curves) and $\Delta\alpha = 2$ (bottom curves). The SEDs have been normalized at $1 \mu\text{m}$ on an arbitrary flux scale. The extinction curves used are those of the Galaxy (Cardelli et al. 1989; *light solid* line), the SMC (Bouchet et al. 1985; *short dashed* line), and the empirical curve for starburst galaxies (Calzetti et al. 1994; *long dashed* line).